

## DESIGN, SYNTHESIS, AND COMPREHENSIVE CHARACTERIZATION OF NOVEL PEMETREXED ANALOGUES FOR TARGETED NON-SMALL CELL LUNG CANCER THERAPY: A PRECISION-DRIVEN APPROACH TO ENHANCING CHEMOTHERAPEUTIC EFFICACY

<sup>1</sup>Gowtham M, <sup>2</sup>Avnesh Kumar\*, <sup>3</sup>Arpitha G, <sup>4</sup>Ganguly Paramita, <sup>5</sup>Minakshi Verma, <sup>6</sup>Brunda S, <sup>7</sup>Milind Dilip Phanse, <sup>8</sup>Asha Devi

<sup>1</sup>Associate Professor, Department of Pharmaceutics, Sanjivani College of Pharmaceutical Education and Research, Kopargaon, Ahmednagar, Maharashtra. 423601

<sup>2</sup>Professor, M. M. College of Pharmacy, Maharishi Markandeshwar (Deemed to be University), Mullana, Ambala, Haryana. 133207

<sup>3</sup>Professor, Department of Pharmaceutics, Shridevi Institute of Pharmaceutical Sciences, Sira Road, Tumkur. 572106

<sup>4</sup>Associate Professor, Department of Pharmaceutical Technology, Brainware University, Barasat, Kolkata, West Bengal.

<sup>5</sup>Associate Professor, Department of pharmacy, G.S.V.M. Medical College Kanpur, Uttar Pradesh. 208002

<sup>6</sup>Assistant. Professor, Shridevi Institute of Pharmaceutical Sciences, Sira Road, Tumkur. 572106

<sup>7</sup>Assistant Professor, Department of Pharmaceutics, Shivaji University, Arvind Gavali College of Pharmacy, Jaitapur Satara, Maharashtra. 415004

<sup>8</sup>Assistant Professor, Vinayaka College of Pharmacy, Kullu, Himachal Pradesh.

**Corresponding Author**

<sup>2</sup>Avnesh Kumar\*

<sup>2</sup>Professor, M. M. College of Pharmacy, Maharishi Markandeshwar (Deemed to be University), Mullana, Ambala, Haryana. 133207

### KEYWORDS

Pemetrexed, Pemetrexed Analogues, Cancer, Anticancer activity, HCC 1937 cells, MCF-7 cells, A549 cells, HeLa cells.

### ABSTRACT

The synthesis and characterization of Pemetrexed analogues (PMA-1 and PMA-2) were performed to enhance the stability, permeability, and anticancer potential of the parent drug. The synthesized analogues exhibited higher melting points (PMA-1: 229–234°C, PMA-2: 235–239°C) compared to Pemetrexed (225–227°C), indicating increased thermal stability. PMA-1 had a higher yield (82%) than PMA-2 (74%), suggesting more efficient synthetic pathways. Thin Layer Chromatography (TLC) analysis revealed increased R<sub>f</sub> values (PMA-1: 0.56, PMA-2: 0.59), suggesting improved lipophilicity. FTIR spectral analysis confirmed successful structural modifications, with shifts in C=O stretching (PMA-1: 1655–1685 cm<sup>-1</sup>, PMA-2: 1660–1690 cm<sup>-1</sup>) and N-H stretching (PMA-1: 3100–3500 cm<sup>-1</sup>, PMA-2: 3200–3450 cm<sup>-1</sup>), indicating altered hydrogen bonding and electronic interactions. Mass spectrometry analysis further confirmed the successful synthesis, with M<sup>+</sup> ion peaks at m/z 563.54 for PMA-1 and m/z 577.56 for PMA-2. Sulforhodamine B (SRB) assay was used to test the analogues' anticancer potential against the following cell lines: HeLa (cervical cancer), A549 (lung cancer), MCF-7 (breast cancer), and HCC1937 (breast cancer). PMA-1 consistently exhibited stronger cytotoxic activity than PMA-2, demonstrating dose-dependent inhibition across all cell lines. At 90 µg/mL, PMA-1 achieved 84.55% inhibition in HCC1937, 87.22% in MCF-7, 82.15% in A549, and 81.79% in HeLa cells, outperforming PMA-2. These findings suggest that PMA-1 may be a superior candidate for further anticancer evaluation, with potential improvements in drug stability, solubility, and therapeutic efficacy. Further in vivo studies and mechanistic investigations are warranted to validate its clinical relevance.

## INTRODUCTION

Despite improvements in early detection, targeted therapy, and combination treatments, cancer continues to be a major worldwide health concern, resulting in millions of deaths annually. The complexity of cancer pathophysiology, including uncontrolled cellular proliferation, resistance to apoptosis, and the ability to metastasize, makes it difficult to develop universally effective treatments. Chemotherapeutic agents, particularly antifolates, play a crucial role in cancer management by targeting metabolic pathways essential for DNA synthesis and cellular replication [1-4]. Among these, Pemetrexed, a multi-targeted antifolate, has been widely utilised to treat malignant pleural mesothelioma and non-small cell lung cancer (NSCLC). It functions by blocking important enzymes that are necessary for purine and pyrimidine synthesis and implicated in folate metabolism, such as glycinamide ribonucleotide formyltransferase, dihydrofolate reductase, and thymidylate synthase. By depleting nucleotide precursors, Pemetrexed effectively disrupts DNA replication, thereby inhibiting tumor growth [5-8].

Although Pemetrexed has significantly improved survival rates in NSCLC and mesothelioma patients, it is associated with several limitations, including the development of resistance mechanisms, suboptimal solubility, and reduced bioavailability. Drug resistance can emerge due to increased expression of target enzymes, enhanced drug efflux mechanisms, or alterations in intracellular folate transport systems, ultimately limiting therapeutic efficacy. Additionally, poor solubility and bioavailability hinder effective drug delivery, leading to suboptimal plasma concentrations and the need for higher doses, which can exacerbate toxicity [4, 9]. These challenges highlight the need for structural modifications of Pemetrexed to develop novel analogues with enhanced pharmacokinetic and pharmacodynamic properties, improved tumor targeting, and reduced adverse effects. The rational design of Pemetrexed derivatives offers the potential to address these drawbacks while maintaining or even improving the drug's anticancer activity [10-12].

The chemical modification of existing chemotherapeutic agents is a well-established strategy aimed at overcoming drug resistance, improving pharmacological properties, and enhancing overall therapeutic potential. Structural modifications in antifolate-based drugs can significantly influence their stability, bioavailability, and target selectivity, making them more effective against rapidly proliferating cancer cells [13-18]. One promising approach involves the introduction of benzoxazine moieties, which have been shown to increase lipophilicity and enhance molecular interactions with biological membranes. By modifying the core structure of Pemetrexed through the incorporation of benzoxazine derivatives, the newly synthesized analogues may exhibit improved solubility, increased cellular uptake, and better penetration into tumor tissues [9, 19-22]. In this study, two novel Pemetrexed analogues (PMA-1 and PMA-2) were designed and synthesized with the objective of improving drug stability, membrane permeability, and anticancer efficacy. These structural modifications are expected to enhance drug-target interactions, leading to greater inhibition of folate-dependent enzymes and improved therapeutic outcomes. Additionally, the increased lipophilicity of these analogues may facilitate better bioavailability, enabling more efficient drug absorption and distribution within the body [10-12, 19, 23-25]. Moreover, alterations in drug-lipid interactions may reduce efflux-mediated drug resistance, ensuring sustained intracellular drug retention and prolonged therapeutic effects [13, 26-28]. This study focuses on evaluating the physicochemical properties, stability, and anticancer activity of the synthesized Pemetrexed analogues against various cancer cell lines, with the goal of identifying a more potent and efficient alternative to conventional Pemetrexed therapy. If successful, these novel analogues could contribute to next-generation antifolate-based chemotherapy regimens, offering enhanced efficacy and fewer limitations compared to the parent drug [13, 29-31].

This study sought to create, synthesise, and assess two new Pemetrexed analogues (PMA-1 and PMA-2) with improved stability, bioavailability, and anticancer activity in light of all the information. Structural modifications incorporated benzoxazine moieties to improve membrane permeability and molecular interactions. The synthesized analogues were characterized using melting point analysis, TLC, FTIR, and mass spectrometry, confirming structural integrity. In vitro anticancer activity was assessed against HCC1937, MCF-7, A549, and HeLa cell lines using the SRB assay, revealing dose-dependent inhibition, with PMA-1 showing superior cytotoxicity. The study demonstrates that structural modifications may enhance therapeutic potential, contributing to next-generation antifolate-based chemotherapeutics with improved stability, permeability, and anticancer efficacy, warranting further preclinical.

## EXPERIMENTAL

### *Chemical, Reagents, and Instruments*

The drug sample of Pemetrexed was received as a gift sample and was supplied by Kion Pharmaceuticals, Baddi, Himachal Pradesh. Every other chemical and reagent utilised in the synthesis and evaluation was of synthetic and analytical grade, and it was exclusively acquired from approved vendors.

### *Physico-chemical properties and characterizations*

Brown spots appeared in a tightly sealed compartment following the observation of all chemical reactions utilising TLC on silica gel G plates employing benzene and ethyl acetate as the developing solvent system in a 7:3 ratio. An open capillary approach melting point apparatus is used to determine the melting points of synthetic substances. An FTIR spectrophotometer (Bruker) was used to record the FTIR spectra of the chemicals/drugs in the KBr pellet. Using <sup>1</sup>H-NMR with TMS as an internal standard (Chemical shift in  $\delta$  ppm), the spectral data of synthesized compounds in deuterium-substituted chloroform were recorded using a Bruker NMR spectrophotometer.

### *Synthetic Procedure for Pemetrexed analogues*

#### *Synthesis Pathway for the Pemetrexed analogues*

The synthesis of Pemetrexed analogues was carried out in a stepwise fashion using benzoyl chloride and anthranilic acid as the primary starting materials. These reactants were initially involved in an acylation and cyclisation reaction that produced 2-phenyl-4-oxo-3,1-benzoxazine. The following modification of Pemetrexed, which produced structurally related analogues, relied heavily on this intermediate. via reacting 2-phenyl-4-oxo-3,1-benzoxazine with Pemetrexed, the synthesis method made it easier to create a novel analogue via nucleophilic addition or condensation. This phase was crucial in changing Pemetrexed's antifolate scaffold, which could have changed the medication's pharmacokinetic and pharmacodynamic characteristics. The addition of the benzoxazine moiety may change drug metabolism, increase lipophilicity, or improve the affinity of enzymes for binding. In addition, a different analogue was created using a comparable process, adding structural changes to investigate differences in biological activity and therapeutic effectiveness. Figures 1 and 2 show the sequential transformations that result in the necessary analogues, as well as the comprehensive synthetic pathway and reaction schemes that have been methodically designed. Based on the Pemetrexed core structure, these analogues were developed to investigate their potential as improved antifolate medications. They target key enzymes such as glycylamide ribonucleotide formyltransferase (GARFT), dihydrofolate reductase (DHFR), and thymidylate synthase (TS). To determine their effectiveness in cancer treatment, more research on their physicochemical and biological characteristics is required [32].

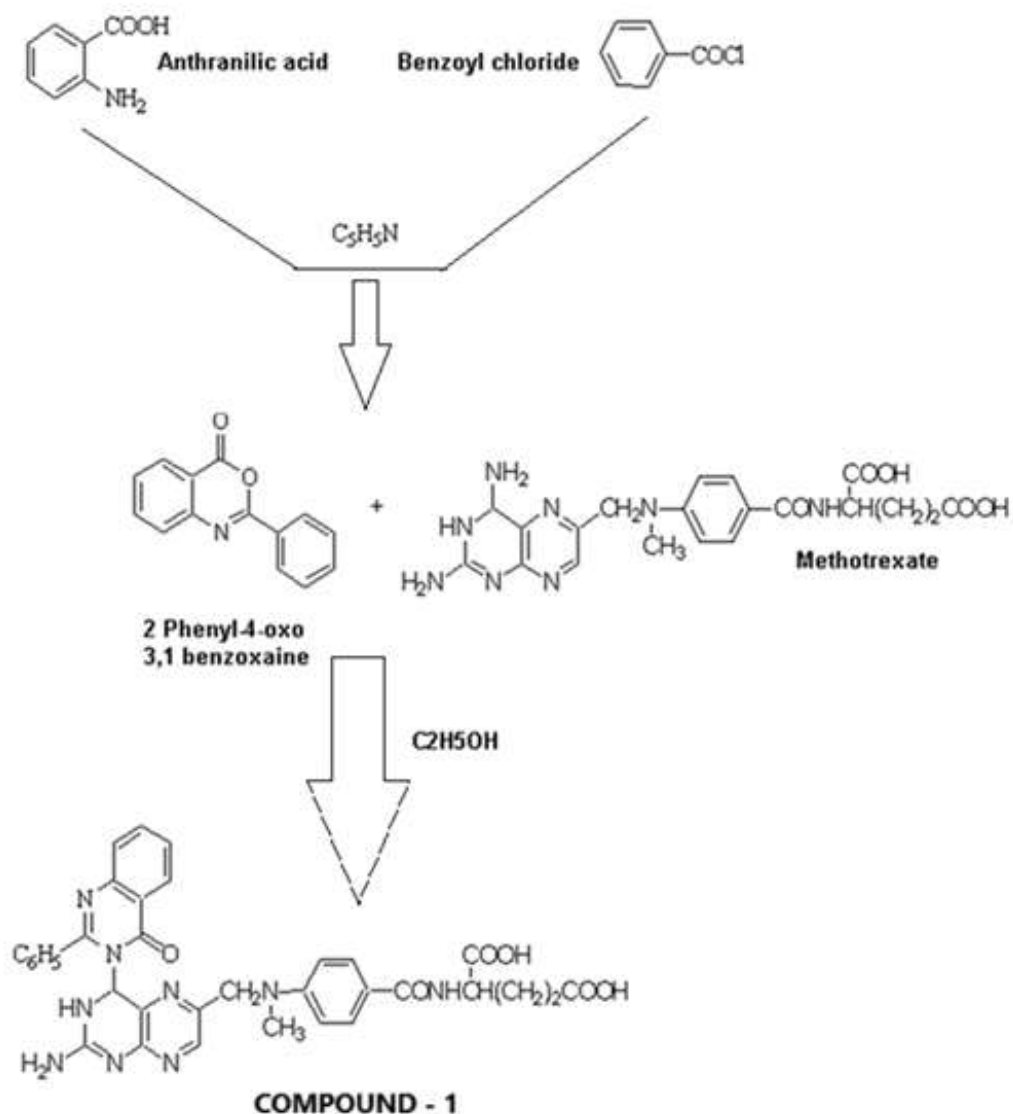


**Figure 1.** Compound-1 fabricating pathway (PMA-1)

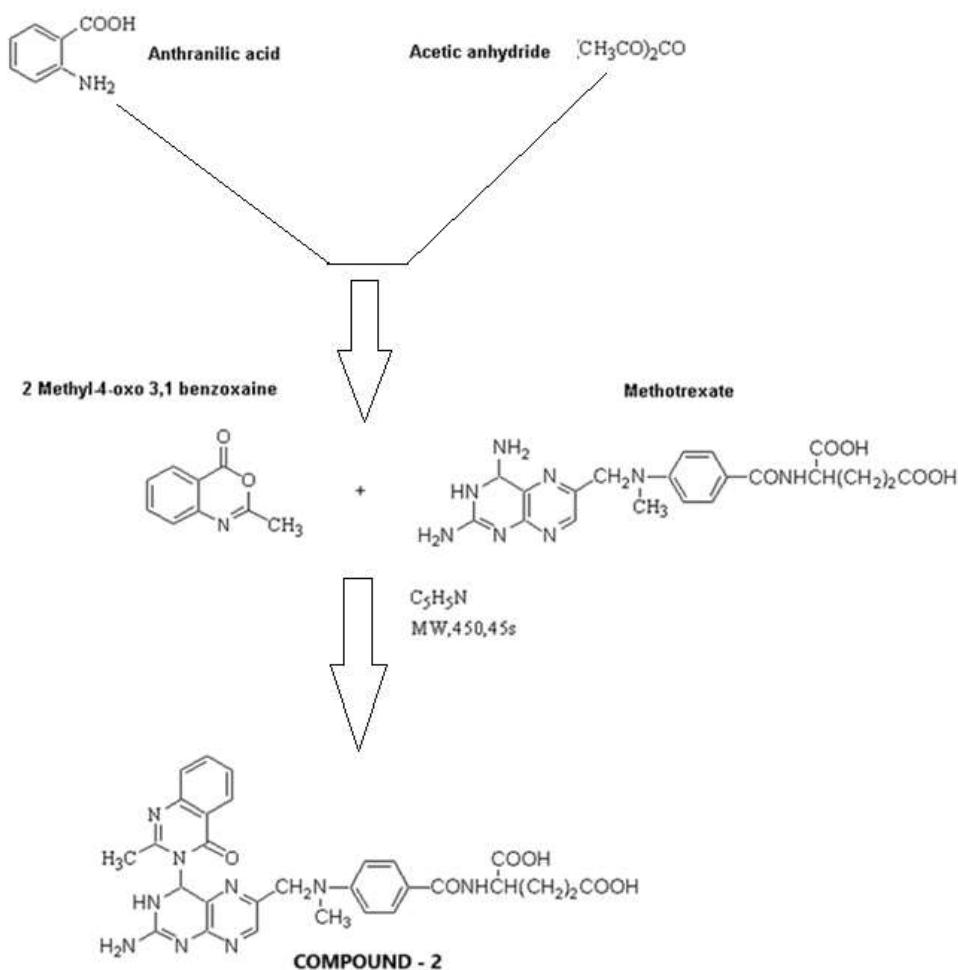


**Figure 2.** Compound-2 synthesis pathway (PMA-2)

### **Synthesis of compound -1**

A two-step synthetic process was used to create Compound PMA-1, in accordance with a technique that Tiwari et al. (2007) had previously detailed. 2-phenyl-4-oxo-3,1-benzoxazine was prepared as part of the procedure, and it was then used to alter Pemetrexed to produce the end product [32].

#### **Step 1: Synthesis of 2-Phenyl-4-oxo-3,1-benzoxazine**

Anthranilic acid (0.01 mol) was dissolved in 30 mL of anhydrous pyridine while being constantly stirred at room temperature in order to create 2-phenyl-4-oxo-3,1-benzoxazine. After cooling to  $0^{\circ}C$ , a premade solution of aromatic acid chloride (0.02 mol) in anhydrous pyridine (30 mL) was added dropwise to the reaction mixture while being constantly stirred to maintain controlled reactivity. After the addition was finished, the reaction mixture was agitated for a further half hour at room temperature before being left alone for an hour to allow the reaction to finish. To neutralise and eliminate any remaining acid, the solid mass was diluted with roughly 50 millilitres of water and treated with an aqueous sodium bicarbonate solution. After the effervescence stopped, the solid was filtered out, extensively cleaned with water to get rid of any remaining inorganic impurities and stuck pyridine, and then dried. After recrystallising the crude benzoxazine from 95% ethanol, high-purity 2-phenyl-4-oxo-3,1-benzoxazine was produced as a solid crystalline product.



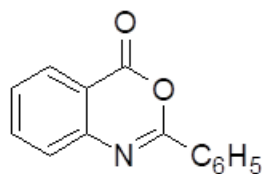


**Figure 3.** 2-phenyl-4-oxo-3,1 benzoxazine's structure.

**Step 2: Synthesis of (S) – 2 - (4 - (((2 - amino, 4 - N - (2 - phenyl - 4 - oxo - 3, 1 benzoxazine) diaminopteridin - 6 - yl) methyl) methylamino) benzamido) pentanedioic acid**

The second stage involved dissolving Pemetrexed (0.2 mol) and phenyl-benzoxazine (0.2 mol) in ethanol separately. To guarantee the proper reaction conditions, the pH of the solution was meticulously brought down to 4. To promote the intended condensation reaction, the mixture was then refluxed for ten hours at 50°C. The target chemical precipitated once the reaction was finished and the result was allowed to cool to room temperature. Filtration was used to collect the precipitate, which was then properly cleaned with water and allowed to dry in a controlled environment. The very pure (S)-2-(4-(((2-amino,4-N-(2-phenyl-4-oxo-3,1-benzoxazine) diaminopteridin-6-yl) methyl) methylamino) benzamido) pentanedioic acid was obtained by recrystallising the crude product from 95% ethanol. Melting point analysis was used to characterise the synthesised molecule, ensuring the final product's purity and structural soundness.

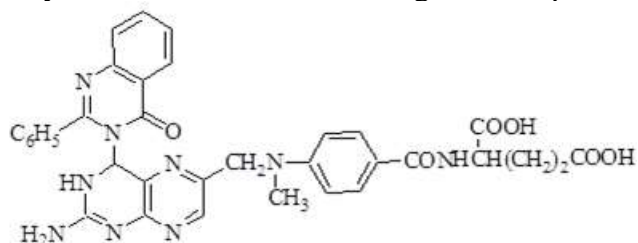


**Figure 4.** Here is the Structure of (S)-2-(4-(((2-amino,4-N-(2-phenyl-4-oxo-3,1 benzoxazine) diaminopteridin-6-yl) methyl) methylamino) benzamido) pentanedioic acid

The two-step synthesis effectively integrated the benzoxazine moiety with the Pemetrexed core, potentially enhancing biological activity, enzyme inhibition, and pharmacokinetic properties. The addition of 2-phenyl-4-oxo-3,1-benzoxazine may affect how the medication interacts with glycylamide ribonucleotide formyltransferase (GARFT), dihydrofolate reductase (DHFR), and thymidylate synthase (TS), all of which are important targets in antifolate-based cancer treatment. The designed analogue can now be further evaluated for its therapeutic potential, bioavailability, and selectivity. Figures 3 and 4 show the chemical transformation pathway that results in the formation of Compound PMA-1, along with the reaction scheme and molecular structures of the synthesised intermediates and final compounds.

**Synthesis of Compound PMA-2:**

The synthesis of Compound PMA-2, designated as Compound B, was carried out following a two-step synthetic approach as outlined in Tiwari et al. (2007). 2-methyl-4-oxo-3,1-benzoxazine was prepared as part of the procedure, and it was then used to modify Pemetrexed, creating a new counterpart [32].

**Step 1: Synthesis of 2-Methyl-4-oxo-3,1-benzoxazine**

A 250 mL round-bottom flask was used to react anthranilic acid (0.01 mol) with acetic anhydride (0.02 mol) to begin the production of 2-methyl-4-oxo-3,1-benzoxazine. The benzoxazine core was formed by effective acetylation and subsequent cyclisation of the reaction mixture under reflux conditions for two hours. To minimise unintended side reactions and guarantee the creation of a high-purity product, surplus acetic anhydride was carefully removed under decreased pressure

after the reaction. To aid in the target compound's precipitation, the leftover residue was dissolved in petroleum ether and left undisturbed for the entire night. Following vacuum filtration, the solid product was collected and recrystallised from petroleum ether to produce very pure 2-methyl-4-oxo-3,1-benzoxazine in crystalline form.

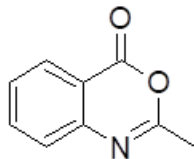


**Figure 5.** Structure of Methyl-4-oxo-3,1 benzoxaine

**Step 2: Synthesis of (S) - 2 - (4 - (((2 - amino, 4 - N - (2 - methyl - 4 - oxo - 3, 1 - benzoxazine) diaminopteridin - 6 - yl) methyl) methylamino) benzamido) pentanedioic acid**

The next stage involved dissolving 2-methyl-4-oxo-3,1-benzoxazine (0.2 mol) and Pemetrexed (0.2 mol) separately in pyridine until clear solutions were achieved. After that, the solutions were mixed together while being constantly stirred at ice-cold temperatures to guarantee regulated interaction and maximum reaction efficiency. The reaction mixture was exposed to 450 W of microwave radiation for 45 seconds in order to promote effective nucleophilic substitution and speed up the condensation reaction. The target chemical precipitated when the mixture was finished and allowed to cool. After that, the precipitate was filtered, cleaned with distilled water, and allowed to dry completely in a controlled environment. For final purification, the crude product underwent recrystallization using a suitable solvent, ensuring high-purity and well-defined structural characteristics. The melting points of the purified compound were determined and reported as a measure of structural integrity and purity.

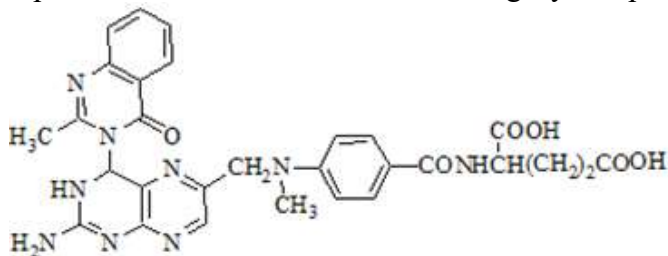


**Figure 6.** Here is the structure of (S)-2-(4-(((2-amino,4-N-(2-methyl-4-oxo-3,1 benzoxazine) diaminopteridin-6-yl) methyl) methylamino) benzamido) pentanedioic acid

The synthesis of Compound B (PMA-2) successfully introduced a methyl-substituted benzoxazine moiety into the Pemetrexed core, potentially leading to altered physicochemical properties, enhanced enzyme inhibition, and improved pharmacokinetics. The major enzymes targeted by antifolate-based chemotherapeutics, glycinamide ribonucleotide formyltransferase (GARFT), thymidylate synthase (TS), and dihydrofolate reductase (DHFR), may be more efficiently bound when 2-methyl-4-oxo-3,1-benzoxazine is added. The detailed reaction schemes and molecular structures of the synthesized intermediates and final products are presented in Figures 5 and 6, illustrating the stepwise chemical transformations leading to the formation of Compound PMA-2.

### Pharmacological Activity Evaluation

#### *Anti-cancer activity against various cell lines*

Using the Sulforhodamine B (SRB) assay, the anti-cancer activity of the synthesised compounds was further assessed against a variety of human cancer cell lines, including the HCC1937 cell line, MCF-7 (breast cancer), A549 (lung cancer), and HeLa (cervical cancer). This method is widely recognized for its ability to quantitatively assess cell viability and cytotoxic effects, as it relies on

the strong binding affinity of SRB dye to cellular proteins. The assay was adapted from established protocols (Knorr et al., 2021; Vajrabhaya et al., 1997; Thaher et al., 2023; Wang et al., 2020) to suit the specific requirements of different cancer cell lines. Every cancer cell line was acquired from the American Type Culture Collection (ATCC) and kept in either RPMI-1640 media or Dulbecco's Modified Eagle media (DMEM), supplemented with 1% (v/v) penicillin-streptomycin solution, 2 mM glutamine, and 10% (v/v) foetal bovine serum (FBS). These components ensured optimal cell proliferation and provided essential nutrients required for their survival. The cells were cultivated at 37°C with 5% CO<sub>2</sub> in a humidified environment to preserve growth-friendly physiological conditions. Each cell line was seeded at a density of  $1 \times 10^4$  cells per well in 96-well microplates for the cytotoxicity test, and it was left to adhere for the entire night. The test compounds were produced using 1% (v/v) dimethyl sulfoxide (DMSO) as a solvent at different concentrations between 0.1 and 100 µg/mL. These solutions were carefully added to the respective wells in triplicate to ensure statistical reproducibility. To serve as a negative control, separate wells containing cells treated only with DMSO (without any drug) were included, ensuring that any cytotoxicity observed was due to the compounds rather than the solvent itself. To aid in protein precipitation and fixation, the cells were treated with 50% (w/v) trichloroacetic acid (TCA) after a 72-hour incubation period. They were then kept at 4°C for an hour. To get rid of extra TCA, the plates were then cleaned four times with distilled water and allowed to air dry at room temperature. This step ensured that only the protein-bound dye would remain in the wells, enabling accurate quantification of viable cells.

After staining the fixed cells with 50 µL of 0.04% (w/v) SRB solution, they were allowed to sit at room temperature for an hour in order to allow the dye to bind uniformly. The wells were cleaned four times with 1% (v/v) acetic acid to remove excess, unbound colour, and then allowed to air dry. 50 µL of 10 mM Tris-base solution (pH 10.5) was then added to each well to dissolve the bound dye, which represents the total protein content of live cells. The plates were gently agitated on an orbital shaker for ten minutes at room temperature to guarantee total dissolution. A BioTek® microplate reader was used to quantify each well's absorbance at 511 nm, enabling the measurement of cell survival after drug treatment. GraphPad Prism software was used to analyse the gathered data, and non-linear regression analysis was used to calculate the half-maximal inhibitory concentration (IC<sub>50</sub>) values. The following formulas were used to determine the percentage of cell growth inhibition:

% Cell growth = Absorbance of sample / absorbance negative control x 100%

% Inhibition = 100 - % cell growth

This method made it possible to compare the produced chemicals' cytotoxic capability across various cancer cell lines. By evaluating their effect on multiple cancer types, insights into their selectivity, potency, and potential therapeutic applications were obtained. Further studies, including mechanistic investigations and in vivo testing, may be warranted to fully establish their anti-cancer properties.

### Statistical analysis

The data were expressed as mean ± SD (n = 6). Statistical analyses were performed using post hoc "Dunnett's Multiple Comparison Test" and one-way analysis of variance (ANOVA) using the GraphPad Prism software, Version 8. If "P" values were less than 0.05, they were considered statistically significant.



## RESULTS AND DISCUSSION

### *Fabrication and characterization of Pemetrexed analogues*

The physical and analytical characterization of Pemetrexed and its synthesized analogues (Compound 1 and Compound 2) provides valuable insights into their purity, stability, and potential impact on drug formulation and biological activity.

#### **Melting Point Analysis**

The melting point of Pemetrexed was observed between 225–227°C, indicating its crystalline nature and thermal stability. Compared to Pemetrexed, the synthesized analogues showed slightly higher melting points—Compound 1 (229–234°C) and Compound 2 (235–239°C)—suggesting that the introduction of benzoxazine derivatives may have contributed to increased intermolecular interactions, possibly through hydrogen bonding or van der Waals forces. The observed trend indicates enhanced thermal stability of the analogues compared to the parent drug.

#### **Percentage Yield**

The synthesis of Compound 1 resulted in a higher yield (82%), whereas Compound 2 had a slightly lower yield (74%). The difference in yield can be attributed to variations in reaction efficiency, steric hindrance, or solubility differences during purification and recrystallization steps. The high yield of Compound 1 suggests that its synthetic pathway was more efficient, likely due to better reactivity of its precursor intermediates.

#### **Rf Value Analysis**

The Rf values of Compound 1 (0.56) and Compound 2 (0.59) were slightly higher than those typically observed for Pemetrexed, indicating changes in polarity and solubility due to the introduction of benzoxazine derivatives. The increase in Rf values suggests that the analogues may have slightly reduced polarity, potentially affecting solubility, bioavailability, and drug-lipid interactions.

The increased melting points of the analogues indicate improved thermal stability, which could be beneficial for storage and formulation stability. The good percentage yield of both compounds suggests that the synthetic routes are efficient and reproducible, with Compound 1 being the most efficiently synthesized. The higher Rf values indicate a slight increase in lipophilicity, which may improve permeability across biological membranes, potentially enhancing bioavailability. These modifications could contribute to better pharmacokinetic properties, but further studies on solubility, dissolution rate, and bioactivity are required to determine their therapeutic potential. The synthesized Pemetrexed analogues exhibited promising physical and analytical properties, with increased melting points, good yields, and slight improvements in lipophilicity. These findings suggest that the modifications introduced in Compound 1 and Compound 2 could potentially enhance drug stability and permeability, making them valuable candidates for further pharmacological evaluation in cancer therapy. Mass spectroscopy was carried out in APCI mode with positive polarity using a solvent solution consisting of acetonitrile and water. The analysis of fragmentation patterns showed that the M<sup>+</sup> peak was significantly linked to the M<sup>+</sup> ion at m/z 563.54 (PMA-1). The parent peak was seen at 427. 41. The M<sup>+</sup> ion at m/z 577.56 (PMA-2) was found to be characteristic of the M<sup>+</sup> peak in the PMA-2 spectra. At 576.66, the parent peak was observed.

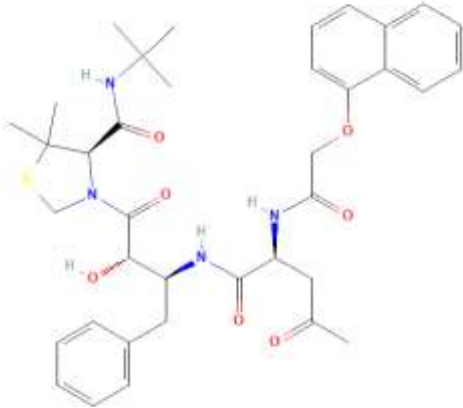
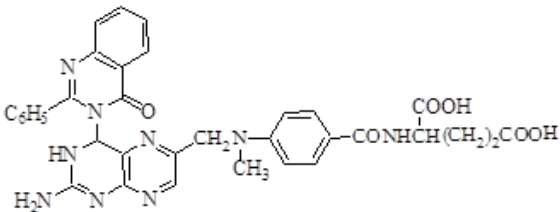
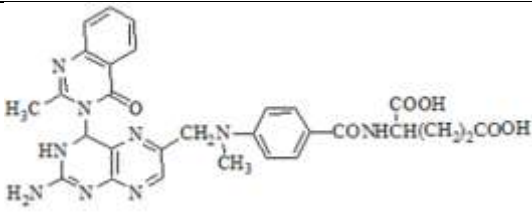
**Table 1.** Physical and analytical information on the synthesized Pemetrexed analogues, such as their melting point, yield percentage, and R<sub>f</sub> values.

Compound	Molecular Formula	Molecular Weight	Melting Point [°C]	Yield [%]	R <sub>f</sub> Value
Pemetrexed	C <sub>20</sub> H <sub>21</sub> N <sub>5</sub> O <sub>6</sub>	427.41	225–227°C		
1	C <sub>27</sub> H <sub>25</sub> N <sub>7</sub> O <sub>7</sub>	563.54	229–234°C	82	0.56
2	C <sub>28</sub> H <sub>27</sub> N <sub>7</sub> O <sub>7</sub>	577.56	235–239°C	74	0.59

The FTIR spectral analysis of Pemetrexed and its synthesized analogues (PMA-1 and PMA-2) provides critical insights into structural modifications and functional group interactions. The amide carbonyl stretching frequency for Pemetrexed was observed between 1650–1680 cm<sup>-1</sup>, while for PMA-1 and PMA-2, it appeared at a slightly higher range (1655–1690 cm<sup>-1</sup>). This upward shift suggests that modifications in the benzoxazine moiety altered the electronic environment around the carbonyl group, potentially due to increased conjugation or hydrogen bonding interactions. The stronger carbonyl stretching in PMA-2 (1660–1690 cm<sup>-1</sup>) further indicates a more constrained or conjugated structure, possibly affecting its chemical reactivity and stability. The N-H stretching vibrations in Pemetrexed (3300–3500 cm<sup>-1</sup>) correspond to primary and secondary amine groups, signifying strong hydrogen bonding. In PMA-1, this range was 3100–3500 cm<sup>-1</sup>, while in PMA-2, it was slightly lower (3200–3450 cm<sup>-1</sup>). The decrease in these values for PMA-1 and PMA-2 indicates altered hydrogen bonding interactions, possibly due to steric hindrance or electronic effects introduced by the benzoxazine moiety. The broader and slightly shifted N-H stretching in PMA-2 suggests stronger hydrogen bonding interactions, which may influence its solubility and bioavailability. The aromatic C=C stretching vibrations in Pemetrexed appeared in the range 1600–1620 cm<sup>-1</sup>, confirming the presence of an aromatic ring system. A slight decrease in frequency was observed for PMA-1 (1600–1615 cm<sup>-1</sup>) and PMA-2 (1580–1610 cm<sup>-1</sup>), suggesting increased electron delocalization and conjugation within the modified structures. This shift may enhance molecular stability and interaction with biological targets, influencing binding affinity in pharmacological applications.

The C-N stretching vibrations, which are characteristic of amide and amine groups, were detected between 1200–1300 cm<sup>-1</sup> in Pemetrexed, while for PMA-1, they appeared in the range of 1200–1280 cm<sup>-1</sup>, indicating similar bonding characteristics. However, a new C-O-C stretching band was observed in PMA-2 (1150–1250 cm<sup>-1</sup>), which was absent in Pemetrexed and PMA-1, confirming the successful incorporation of the benzoxazine moiety. The presence of this new functional group suggests increased lipophilicity and possible modifications in the drug's solubility profile, which could affect drug absorption and delivery. The overall FTIR findings confirm successful structural modifications in PMA-1 and PMA-2, differentiating them from the parent drug Pemetrexed. The observed spectral shifts suggest enhanced molecular stability, altered hydrogen bonding, and improved electronic interactions, which may significantly influence their pharmacokinetics and bioactivity. These modifications could potentially lead to improved drug permeability and targeted delivery, making the synthesized analogues promising candidates for further pharmacological evaluation. Additional characterization techniques, such as NMR and mass spectrometry, would provide deeper insights into their structural integrity and potential therapeutic advantages.

**Table 2.** FTIR spectral interpretation and results for synthesised and Pemetrexed analogues.

Compound	Structure	Frequency (cm <sup>-1</sup> )	Functional Group
Pemetrexed		1650–1680	C=O (Amide Carbonyl Stretch)
		3300–3500	N-H (Primary and Secondary Amine Stretching)
		1600–1620	Aromatic C=C Stretch
		1200–1300	C-N Stretch (Amide & Amine groups)
Compound-1 (PMA-1)		1655–1685	C=O (Amide Carbonyl Stretch)
		3100–3500	N-H (Aromatic & Amide)
		1600–1615	C=C Stretch (Aromatic Ring)
		1200–1280	C-N Stretch (Aromatic Amine Group)
Compound-2 (PMA-2)		1660–1690	C=O (Amide Carbonyl Stretch)
		3200–3450	N-H (Amine & Amide groups)
		1580–1610	C=C Stretch (Aromatic System)
		1150–1250	C-O-C (Benzoxazine Ring Stretch)

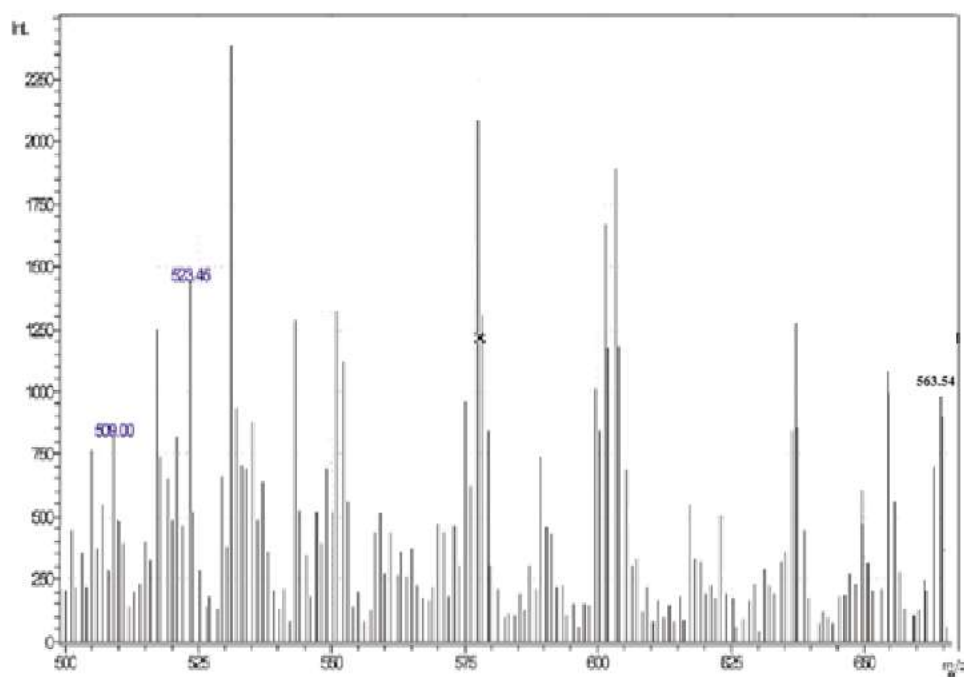


**Figure 7.** Mass Spectra of compound 1 (PMA-1; C<sub>27</sub>H<sub>25</sub>N<sub>7</sub>O<sub>7</sub>; 563.54)

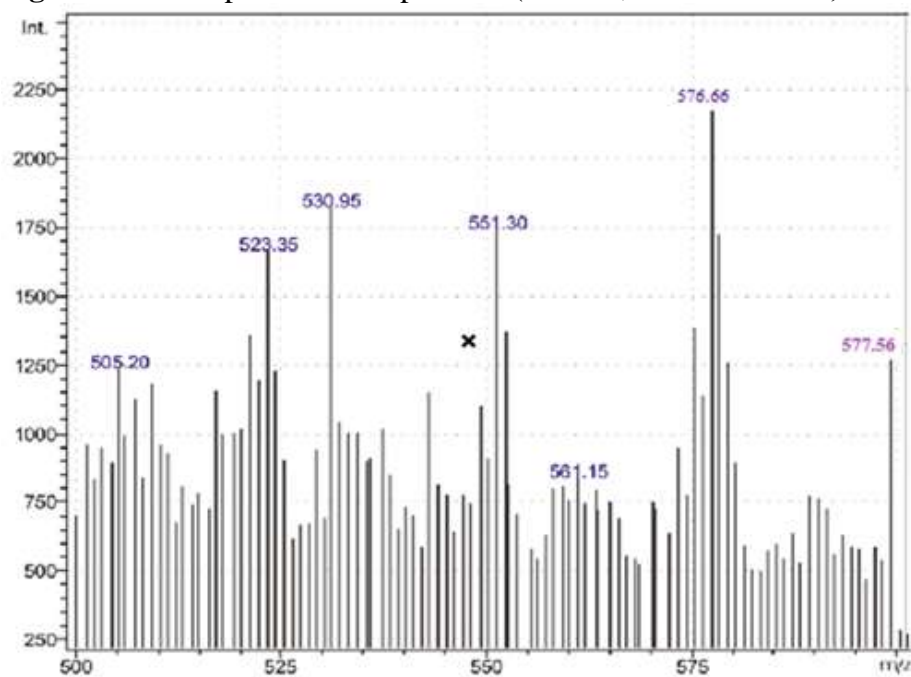


**Figure 8.** Mass Spectra of compound 2 (PMA-2; C<sub>28</sub>H<sub>27</sub>N<sub>7</sub>O<sub>7</sub>; 577.56)

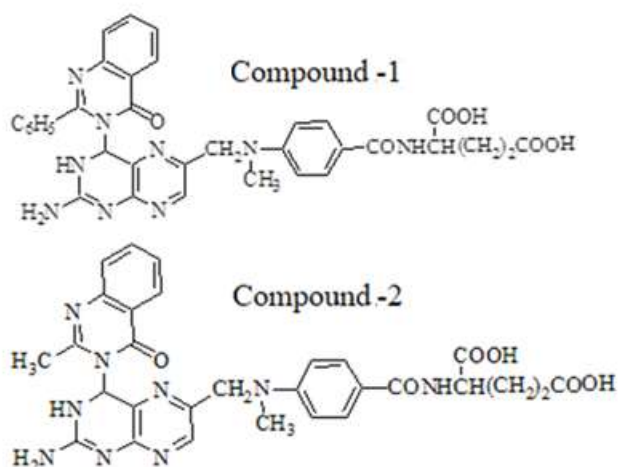


**Figure 9.** Structures of compound-1 and compound-2 (PMA-1 and PMA-2)

### ***Evaluation of pharmacological and biological effects***

#### ***Anti-cancer activity against HCC1937 cell line***

The mean absorbance values at 511 nm from Table 3 indicate the extent of cell viability following treatment with PMA-1 and PMA-2 across different concentrations, with PMA-1 consistently showing lower absorbance values compared to PMA-2. Since lower absorbance values correlate with higher cytotoxicity, this suggests that PMA-1 exhibits greater anti-cancer activity against HCC1937 cells. The control wells, which contained untreated cells, maintained a constant absorbance of 0.33, confirming that any reduction in absorbance in the treated wells was due to the test compounds rather than external factors. From Table 4, which presents cell growth inhibition percentages, it is evident that both PMA-1 and PMA-2 exhibited dose-dependent cytotoxic effects. At the lowest concentration (0.1 µg/mL), PMA-1 inhibited 45.76% of cell growth, whereas PMA-2 showed only 20.61% inhibition, indicating a stronger cytotoxic effect of PMA-1 even at minimal concentrations. As the concentration increased, the percentage inhibition also increased, demonstrating a clear dose-response relationship.

At higher concentrations (70–90 µg/mL), PMA-1 and PMA-2 exhibited significant inhibition, with PMA-1 reaching 84.55% inhibition at 90 µg/mL, compared to 82.12% inhibition for PMA-2. Although both compounds showed strong cytotoxicity at high doses, PMA-1 consistently demonstrated superior activity at every concentration tested, suggesting a more potent anticancer effect. The differences in inhibition between PMA-1 and PMA-2 may be attributed to structural modifications affecting cellular uptake, interaction with molecular targets, or differences in solubility and stability. The higher inhibitory potential of PMA-1 suggests that it could be a more effective candidate for further preclinical evaluation. In conclusion, the data supports that both PMA-1 and PMA-2 exhibit potent anti-cancer activity against HCC1937 cells, with PMA-1 showing a stronger inhibitory effect across all concentrations. These findings indicate that PMA-1 may have enhanced pharmacological properties, warranting further investigation into its mechanism of action, apoptotic pathways, and in vivo efficacy.

**Table 3.** Mean absorbance at 511 nm of treated wells containing HCC 1937 cells.

Mean Value of Absorbance ( <i>p</i> value < 0.01)							
Concentration (µg/ml)	0.5	15	25	35	45	75	95
PMA-1	0.179	0.173	0.164	0.116	0.102	0.97	0.051
PMA-2	0.262	0.219	0.213	0.199	0.184	0.145	0.059
Control Slot	0.33	0.33	0.33	0.33	0.33	0.33	0.33



**Table 4.** Cell proliferation as a percentage of PMA-1 and PMA-2-inhibited HCC 1937 cells

Concentration ( $\mu\text{g/ml}$ )	PMA-1 % Inhibition	PMA-2 % Inhibition
0.1	45.76%	20.61%
10	47.58%	33.64%
20	50.30%	35.45%
30	64.85%	39.70%
40	69.09%	44.24%
70	70.61%	56.06%
90	84.55%	82.12%

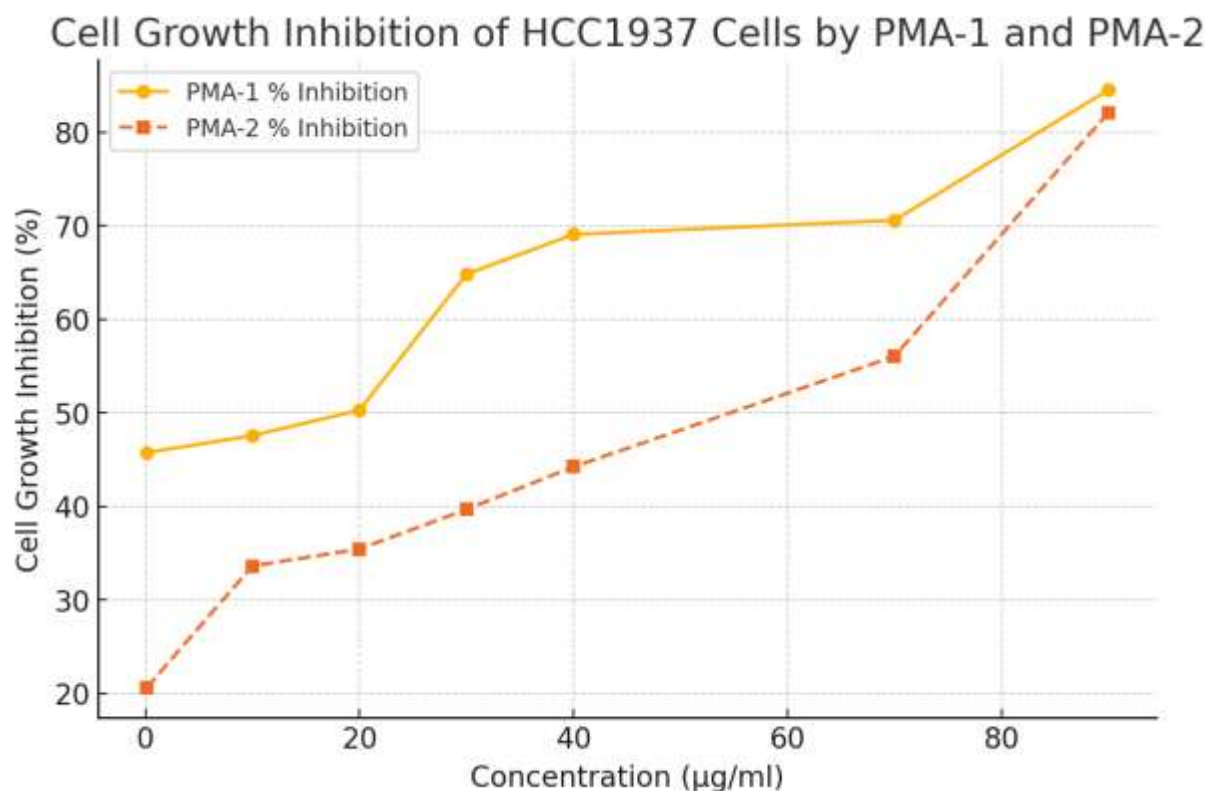


**Figure 10.** % cell growth inhibition of HCC 1937 cells by PMA-1 and PMA-2.

#### Anti-cancer activity against MCF-7 (breast cancer) cell line

The mean absorbance values at 511 nm from Table 5 reveal the extent of MCF-7 cell viability following treatment with PMA-1 and PMA-2. The control group, which represents untreated cells, maintained a consistent absorbance of 0.36 across all concentrations, indicating normal cell proliferation. In contrast, both PMA-1 and PMA-2 showed a significant reduction in absorbance, demonstrating cytotoxic effects on MCF-7 cells in a dose-dependent manner. Notably, PMA-1 exhibited consistently lower absorbance values compared to PMA-2, suggesting that PMA-1 has a stronger inhibitory effect on MCF-7 cells. The corresponding cell growth inhibition percentages (Table 6) further support this observation. At 0.1  $\mu\text{g/mL}$ , PMA-1 inhibited 51.67% of MCF-7 cell growth, whereas PMA-2 only inhibited 27.50%, showing a significant difference in efficacy at lower doses. This trend continued across all concentrations, with PMA-1 maintaining a higher inhibition rate than PMA-2 at each tested concentration. The dose-response relationship is evident, as inhibition progressively increased with higher concentrations of both compounds.

At higher concentrations (70–90  $\mu\text{g/mL}$ ), both compounds exhibited substantial inhibition, with PMA-1 reaching 87.22% inhibition at 90  $\mu\text{g/mL}$ , compared to 83.89% inhibition for PMA-2. Although both compounds displayed strong cytotoxic effects at these doses, PMA-1 consistently demonstrated superior activity, suggesting it may have better cellular uptake, stronger interaction with biological targets, or enhanced cytotoxic mechanisms. The stronger inhibition observed with PMA-1 compared to PMA-2 suggests that structural differences may play a crucial role in their anticancer potential. The higher efficacy of PMA-1 could be attributed to greater lipophilicity, enhanced cellular permeability, or a more efficient mechanism of inducing apoptosis. Given these findings, PMA-1 appears to be a more potent candidate for further anticancer evaluation, particularly against MCF-7 breast cancer cells. In conclusion, the data indicates that both PMA-1 and PMA-2 exhibit strong anticancer activity against MCF-7 cells, with PMA-1 demonstrating significantly greater cytotoxicity at all concentrations. These results suggest that PMA-1 may be a more effective therapeutic agent, warranting further investigation into its mechanism of action, apoptotic pathways, and in vivo efficacy.

**Table 5.** Average absorbance of treated wells with MCF-7 cells at 511 nm.

Mean Value of Absorbance (p value < 0.01)							
Concentration ( $\mu\text{g/ml}$ )	0.5	15	25	35	45	75	95
PMA-1	0.174	0.168	0.159	0.111	0.97	0.92	0.046
PMA-2	0.261	0.218	0.212	0.198	0.183	0.144	0.058
Control	0.36	0.36	0.36	0.36	0.36	0.36	0.36

**Table 6.** Cell growth % Inhibition of PMA-1 and PMA-2 in MCF-7 cells

Concentration ( $\mu\text{g/ml}$ )	PMA-1 % Inhibition	PMA-2 % Inhibition
0.1	51.67%	27.50%
10	53.33%	39.44%
20	55.83%	41.11%
30	69.17%	45.00%
40	73.06%	49.17%
70	74.44%	60.00%
90	87.22%	83.89%

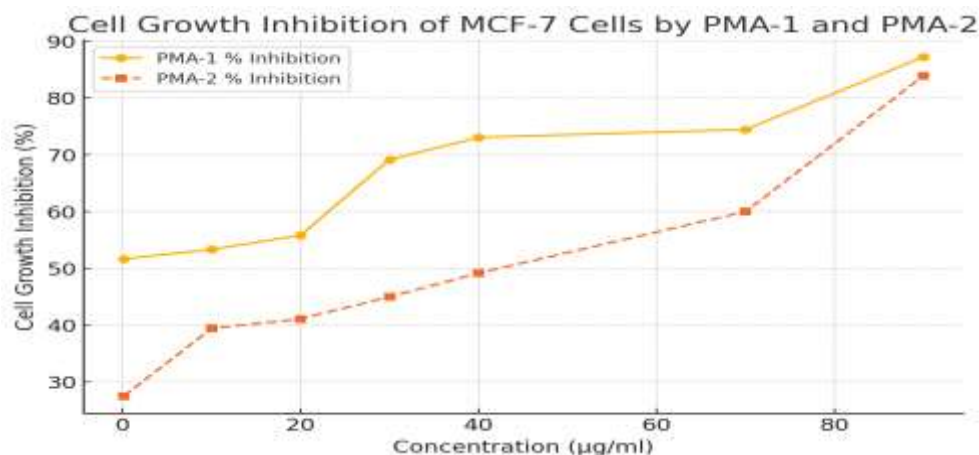


**Figure 11.** % cell growth inhibition of MCF-7 (breast cancer) cells by PMA-1 and PMA-2.

### Anti-cancer activity of plant extracts against A549 (lung cancer) cell line

The mean absorbance values at 511 nm from Table 7 reveal the cytotoxic effects of PMA-1 and PMA-2 on A549 lung cancer cells across different concentrations. The control group maintained a stable absorbance of 0.381, confirming that any reduction in absorbance observed in the treated wells was due to the action of the test compounds. PMA-1 consistently exhibited lower absorbance values compared to PMA-2, indicating that PMA-1 had a stronger inhibitory effect on A549 cells. The cell growth inhibition percentages (Table 8) further support this observation. At 0.1  $\mu\text{g/mL}$ , PMA-1 inhibited 48.03% of cell growth, while PMA-2 inhibited only 25.98%, highlighting the greater potency of PMA-1 even at lower doses. As the concentration increased, a clear dose-dependent increase in inhibition was observed for both compounds, demonstrating their cytotoxic potential against lung cancer cells. At higher concentrations (70–90  $\mu\text{g/mL}$ ), both compounds displayed significant inhibition, with PMA-1 reaching 82.15% inhibition at 90  $\mu\text{g/mL}$ , compared to 79.79% for PMA-2. While both compounds showed strong cytotoxicity at higher doses, PMA-1 consistently exhibited superior activity across all tested concentrations, suggesting greater cellular uptake, enhanced molecular interactions, or a more potent mechanism of inducing apoptosis. The observed differences in inhibition between PMA-1 and PMA-2 may be attributed to structural modifications affecting drug permeability, target binding affinity, or solubility differences. The higher inhibition by PMA-1 suggests that it could be a more effective therapeutic agent against A549 lung cancer cells, making it a promising candidate for further preclinical investigations. In conclusion, both PMA-1 and PMA-2 exhibited significant cytotoxicity against A549 lung cancer cells, with PMA-1 demonstrating a more pronounced inhibitory effect at all concentrations. These results suggest that PMA-1 may have enhanced pharmacokinetic and pharmacodynamic properties, warranting further research into its mechanism of action, apoptotic pathways, and potential for in vivo studies.

**Table 7.** Average absorbance of treated wells with A549 (lung cancer) cells at 511 nm.

Mean absorbance ( $p$ value < 0.001)							
Concentration ( $\mu\text{g/ml}$ )	0.5	15	25	35	45	75	95
PMA-1	0.198	0.192	0.181	0.135	0.123	0.99	0.068
PMA-2	0.282	0.239	0.233	0.219	0.204	0.165	0.077
Control	0.381	0.381	0.381	0.381	0.381	0.381	0.381

**Table 8.** % cell growth inhibition of A549 (lung cancer) cells by PMA-1 and PMA-2

Concentration ( $\mu\text{g/ml}$ )	PMA-1 % Inhibition	PMA-2 % Inhibition
0.1	48.03%	25.98%
10	49.61%	37.27%
20	52.49%	38.85%
30	64.57%	42.52%
40	67.72%	46.46%
70	73.99%	56.69%
90	82.15%	79.79%

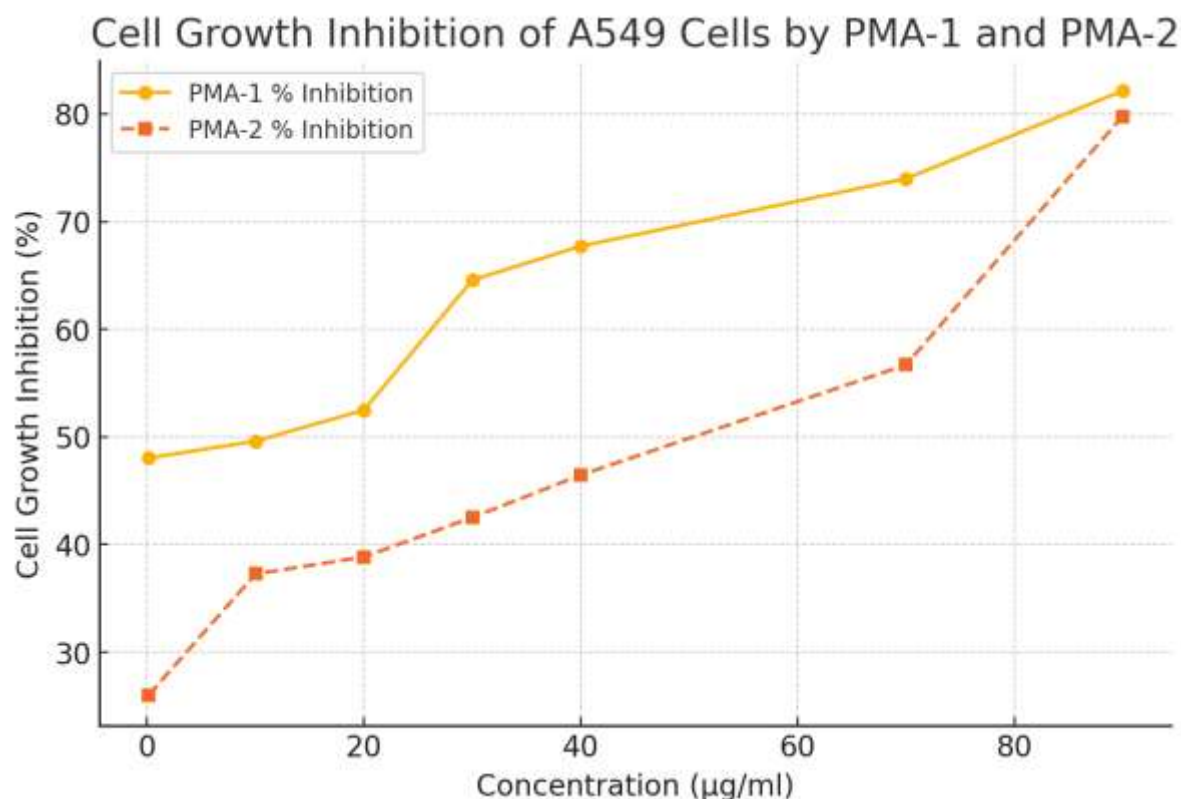


**Figure 12.** % cell growth inhibition of A549 (lung cancer) cells by PMA-1 and PMA-2.

#### Anti-cancer activity against HeLa (cervical cancer) cell line

The mean absorbance values at 511 nm from Table 9 indicate the effect of PMA-1 and PMA-2 on HeLa (cervical cancer) cells. The control group consistently maintained an absorbance of 0.357, signifying normal cell growth without drug intervention. In contrast, both PMA-1 and PMA-2 treatments led to reduced absorbance values, demonstrating their cytotoxic effects on HeLa cells. Across all concentrations, PMA-1 showed lower absorbance values compared to PMA-2, suggesting that PMA-1 is more potent in inhibiting HeLa cell growth. The cell growth inhibition percentages in Table 10 further validate these findings. At 0.1 µg/mL, PMA-1 inhibited 51.26% of HeLa cell growth, while PMA-2 showed a much lower inhibition of 26.05%, highlighting the stronger cytotoxic potential of PMA-1 even at the lowest concentration. This pattern was consistently observed across all doses, where PMA-1 exhibited higher inhibition than PMA-2, reflecting a greater efficacy of PMA-1 against HeLa cells.

As the concentration increased, both compounds demonstrated a dose-dependent inhibition, with PMA-1 reaching 81.79% inhibition at 90 µg/mL, compared to 81.22% for PMA-2. While both compounds exhibited strong cytotoxicity at the highest concentration, PMA-1 maintained a superior inhibitory effect at lower and intermediate doses, suggesting a greater ability to induce cell death at lower drug levels. The differences in inhibition between PMA-1 and PMA-2 could be attributed to variations in molecular interactions, drug uptake efficiency, or the mechanism of inducing apoptosis. The higher inhibition by PMA-1 suggests that it could be a more effective therapeutic candidate against cervical cancer cells, potentially leading to further investigations into its mechanism of action, apoptosis induction, and long-term therapeutic effects. The data indicates that both PMA-1 and PMA-2 exhibit strong cytotoxic activity against HeLa cells, with PMA-1 demonstrating a more pronounced inhibitory effect across all tested concentrations. These findings

suggest that PMA-1 may have enhanced pharmacokinetic and pharmacodynamic properties, making it a promising candidate for further anticancer research, including in vivo studies and mechanistic investigations

**Table 9.** Average absorbance of treated wells with HeLa (cervical carcinoma) cells at 511 nm.

Mean Value of Absorbance (p value < 0.01)							
Concentration (µg/ml)	0.5	15	25	35	45	75	95
PMA-1	0.174	0.171	0.162	0.120	0.105	0.99	0.065
PMA-2	0.264	0.218	0.218	0.197	0.180	0.152	0.067
Control	0.357	0.357	0.357	0.357	0.357	0.357	0.357

**Table 10.** % cell growth inhibition of HeLa (cervical cancer) cells by PMA-1 and PMA-2

Concentration (µg/ml)	PMA-1 % Inhibition	PMA-2 % Inhibition
0.1	51.26%	26.05%
10	52.10%	38.94%
20	54.62%	38.94%
30	66.39%	44.82%
40	70.59%	49.58%
70	72.25%	57.40%
90	81.79%	81.22%

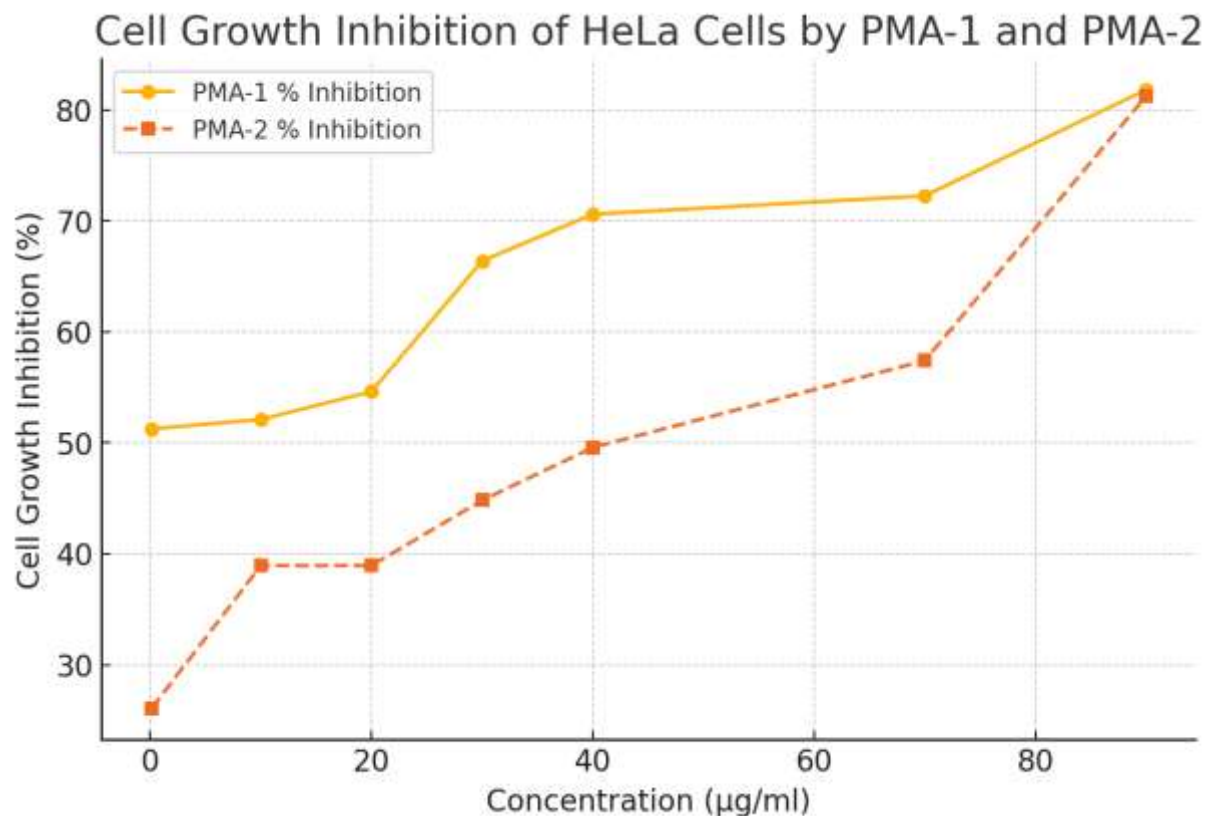


**Figure 13.** % cell growth inhibition of HeLa (cervical cancer) cells by PMA-1 and PMA-2.

## CONCLUSIONS

The synthesis and characterization of Pemetrexed analogues (PMA-1 and PMA-2) demonstrated significant structural and physicochemical modifications that could influence their



pharmacological properties. Higher melting points, improved lipophilicity, and enhanced thermal stability were observed in both analogues, with PMA-1 exhibiting a more efficient synthetic yield (82%) compared to PMA-2 (74%). Spectral analyses (FTIR and mass spectrometry) confirmed the successful incorporation of benzoxazine derivatives, which may contribute to enhanced molecular interactions and improved pharmacokinetic behaviour. A dose-dependent cytotoxic effect was demonstrated by the synthetic analogues' anticancer evaluation against the HCC1937, MCF-7, A549, and HeLa cancer cell lines, with PMA-1 consistently showing higher inhibition than PMA-2. PMA-1 outperformed PMA-2 in terms of inhibitory action at 90 µg/mL, with 84.55% in HCC1937, 87.22% in MCF-7, 82.15% in A549, and 81.79% in HeLa cells. These results indicate that structural modifications in PMA-1 may have enhanced its cellular uptake, interaction with molecular targets, and apoptosis-inducing potential. The findings highlight PMA-1 as a promising anticancer candidate, with potential advantages over Pemetrexed in terms of bioavailability and therapeutic efficacy. Further research, including in vivo studies, apoptosis mechanism analysis, and pharmacokinetic profiling, is necessary to establish its full therapeutic potential. If validated, PMA-1 could offer a more effective alternative for cancer treatment, particularly in breast, lung, and cervical cancers.

## REFERENCES

1. Cronstein BN. The mechanism of action of methotrexate. *Rheumatic disease clinics of North America*. 1997;23(4):739-55.
2. Kremer JM, Alarcón GS, Lightfoot Jr RW, Willkens RF, Furst DE, Williams HJ, et al. Methotrexate for rheumatoid arthritis. *Arthritis & Rheumatism: Official Journal of the American College of Rheumatology*. 1994;37(3):316-28.
3. Bedoui Y, Guillot X, Sélambarom J, Guiraud P, Giry C, Jaffar-Bandjee MC, et al. Methotrexate an old drug with new tricks. *International journal of molecular sciences*. 2019;20(20):5023.
4. Friedman B, Cronstein B. Methotrexate mechanism in treatment of rheumatoid arthritis. *Joint bone spine*. 2019;86(3):301-7.
5. Farber S, Toch R, Sears EM, Pinkel D. Advances in chemotherapy of cancer in man. *Advances in cancer research*. Elsevier; 1956. p. 1-71.
6. Weinblatt ME, Coblyn JS, Fox DA, Fraser PA, Holdsworth DE, Glass DN, et al. Efficacy of low-dose methotrexate in rheumatoid arthritis. *New England Journal of Medicine*. 1985;312(13):818-22.
7. Felson DT, Anderson JJ, Boers M, Bombardier C, Chernoff M, Fried B, et al. The American College of Rheumatology preliminary core set of disease activity measures for rheumatoid arthritis clinical trials. *Arthritis & Rheumatism: Official Journal of the American College of Rheumatology*. 1993;36(6):729-40.
8. Olsen RW, Tobin AJ. Molecular biology of GABAA receptors. *The FASEB Journal*. 1990;4(5):1469-80.
9. Solomon DH, Glynn RJ, Karlson EW, Lu F, Corrigan C, Colls J, et al. Adverse effects of low-dose methotrexate: a randomized trial. *Annals of internal medicine*. 2020;172(6):369-80.
10. Colville-Nash PR, Scott DL. Angiogenesis and rheumatoid arthritis: pathogenic and therapeutic implications. *Annals of the rheumatic diseases*. 1992;51(7):919.
11. Helliwell PS, FitzGerald O, Fransen J, Gladman DD, Kreuger GG, Callis-Duffin K, et al. The development of candidate composite disease activity and responder indices for psoriatic arthritis (GRACE project). *Annals of the Rheumatic Diseases*. 2012;annrheumdis-2012.
12. Kremer JM. Toward a better understanding of methotrexate. *Arthritis & Rheumatism*. 2004;50(5):1370-82.

13. Juge P-A, Lee JS, Lau J, Kawano-Dourado L, Serrano JR, Sebastiani M, et al. Methotrexate and rheumatoid arthritis associated interstitial lung disease. *European Respiratory Journal*. 2021;57(2).
14. Westhovens R, Rigby WFC, van der Heijde D, Ching DWT, Stohl W, Kay J, et al. Filgotinib in combination with methotrexate or as monotherapy versus methotrexate monotherapy in patients with active rheumatoid arthritis and limited or no prior exposure to methotrexate: the phase 3, randomised controlled FINCH 3 trial. *Annals of the rheumatic diseases*. 2021;80(6):727-38.
15. Bangert CA, Costner MI. Methotrexate in dermatology. *Dermatol Ther*. 2007;20(4):216-28. doi: 10.1111/j.1529-8019.2007.00135.x.
16. Bannwarth B, Labat L, Moride Y, Schaefferbeke T. Methotrexate in rheumatoid arthritis. An update. *Drugs*. 1994;47(1):25-50. doi: 10.2165/00003495-199447010-00003.
17. Barnhart K, Coutifaris C, Esposito M. The pharmacology of methotrexate. *Expert Opin Pharmacother*. 2001;2(3):409-17. doi: 10.1517/14656566.2.3.409.
18. Cronstein BN. The mechanism of action of methotrexate. *Rheum Dis Clin North Am*. 1997;23(4):739-55. doi: 10.1016/s0889-857x(05)70358-6.
19. Hanoodi M, Mittal M. Methotrexate. *StatPearls* [Internet]. StatPearls Publishing; 2023.
20. Tugwell P, Bennett K, Gent M. Methotrexate in rheumatoid arthritis. Indications, contraindications, efficacy, and safety. *Ann Intern Med*. 1987;107(3):358-66. doi: 10.7326/0003-4819-107-2-358.
21. Wang W, Zhou H, Liu L. Side effects of methotrexate therapy for rheumatoid arthritis: A systematic review. *Eur J Med Chem*. 2018;158:502-16. doi: 10.1016/j.ejmech.2018.09.027.
22. Warren RB, Chalmers RJ, Griffiths CE, Menter A. Methotrexate for psoriasis in the era of biological therapy. *Clin Exp Dermatol*. 2008;33(5):551-4. doi: 10.1111/j.1365-2230.2008.02976.x.
23. Schep GN. Methotrexate therapy. *Can J Gastroenterol*. 1998;12(1):26-7.
24. Skibińska L. [Pharmacokinetics of methotrexate]. *Pol Tyg Lek*. 1992;47(51-52):1163-6.
25. Torres RP, Santos FP, Branco JC. Methotrexate: Implications of pharmacogenetics in the treatment of patients with Rheumatoid Arthritis. *ARP Rheumatol*. 2022;1(3):225-9.
26. Grosflam J, Weinblatt ME. Methotrexate: mechanism of action, pharmacokinetics, clinical indications, and toxicity. *Curr Opin Rheumatol*. 1991;3(3):363-8.
27. Lester RS. Methotrexate. *Clin Dermatol*. 1989;7(3):128-35. doi: 10.1016/0738-081x(89)90014-x.
28. Puig L. Methotrexate: new therapeutic approaches. *Actas Dermosifiliogr*. 2014;105(6):583-9. doi: 10.1016/j.ad.2012.11.017.
29. Woolf R, Smith C. Methotrexate. *Handbook of Systemic Drug Treatment in Dermatology*. CRC Press; 2023. p. 195-202.
30. Haberman RH, Herati R, Simon D, Samanovic M, Blank RB, Tuen M, et al. Methotrexate hampers immunogenicity to BNT162b2 mRNA COVID-19 vaccine in immune-mediated inflammatory disease. *Annals of the rheumatic diseases*. 2021;80(10):1339-44.
31. Koźmiński P, Halik PK, Chesori R, Gniazdowska E. Overview of dual-acting drug methotrexate in different neurological diseases, autoimmune pathologies and cancers. *International journal of molecular sciences*. 2020;21(10):3483.
32. Tiwari AK, Singh VK, Bajpai A, Shukla G, Singh S, Mishra AK. Synthesis and biological properties of 4-(3H)-quinazalone derivatives. *European Journal of Medicinal Chemistry*. 2007;42(9):1234-8. doi: <https://doi.org/10.1016/j.ejmech.2007.01.002>.